Chapter 4
Mode-Shape Identification of Representative Samples with Digital Image Correlation

Devin Binns, Baiza Mand, Mason Rollans, Peter Beck, Christopher Teti, Kennan Hodovic, and Jim Declerk

Abstract Experimental modal analysis and environmental vibration tests are often used to characterize the modal parameters of a mechanical structure, namely the resonant frequencies, mode shapes, and damping ratios. Typically, these tests rely on attaching sensors to the structure to measure accelerations, which is then processed to extract the modal parameters. There are often testing limitations related to the number of sensors, placement, attachment method, and data acquisition channels needed when using accelerometers. Digital image correlation (DIC) has the potential to replace accelerometers in certain situations; however, there are still questions related to its validity in modal testing and correlation to modal testing performed with accelerometers. In this study, DIC was used to measure displacements in an object for the determination of modal parameters and then compare them to the modal parameters obtained from the traditional method of mounting accelerometers. A flat aluminum plate was tested via impact excitation and results from measurements with DIC were compared to a finite element solution and testing with accelerometer measurements. The measured mode shapes, which qualitatively agreed with both the accelerometer results and the theoretical model, provided higher spatial fidelity than accelerometers. Results produced with DIC measurements yielded natural frequencies with a similar accuracy as accelerometers. Tests with and without accelerometers showed a consistent 3% difference in natural frequencies due to accelerometer mass loading as a source of error.

Keywords Mode shape identification · Experimental modal analysis · Digital Image Correlation (DIC) · Impact testing · Finite Element · Image Processing

List of Notations and Abbreviations: Digital Image Correlation (DIC), Laser Doppler Vibrometry (LDV), Finite Element Analysis (FEA), Data Acquisition Unit (DAQ), Direct Current (DC), Integrated Circuit Piezoelectric (ICP), Transistor-Transistor Logic (TTL), Comma Separated Variable (CSV), Frequency Response Function (FRF), Fast Fourier Transform

Devin Binns
Department of Aerospace and Mechanical Engineering, New Mexico State University, Las Cruces, New Mexico 88003
e-mail: dmbinns@lanl.gov

Baiza Mand
Department of Engineering Physics and Department of Computer Science, Colorado School of Mines, Golden, Colorado 80401
e-mail: mand@lanl.gov

Mason Rollans
Mechanical Engineering Department, Brigham Young University, Provo, Utah 84602
e-mail: mjrollans@lanl.gov

Peter Beck · Christopher Teti
Verification and Validation Division, Los Alamos National Laboratory, Los Alamos, NM 87545
e-mail: pmbeck@lanl.gov

Kennan Hodovic
Engineering Division, Los Alamos National Laboratory, Los Alamos, NM 87545
e-mail: kennan@lanl.gov

Jim Declerk
Department of Mechanical and Aerospace Engineering, Michigan Technological University, Houghton, Michigan 49931
e-mail: jdeclerck@mtu.edu

Kristin B. Zimmerman, PhD (eds.), *Computer Vision and SLDV for Structural Dynamics, 2026, Vol. 6*, Conference Proceedings of the Society for Experimental Mechanics Series, https://doi.org/10.1007/978-8-743-81445-0_4

(FFT), Auto Power Spectrum Density (APSD), Effective Independence Method (EFI), Frames Per Second (FPS), Signal to Noise Ratio (SNR), Modal Assurance Criterion (MAC)

Introduction

Structures in a service environment experience many vibrations and shocks which lead to wear, causing premature failure. As a result, many industries use vibrational testing to qualify and validate components that will be used in a service environment. Commonly, vibrational tests use accelerometers to record and collect a test article's dynamic response. These sensors can distort results due to the additional mass of the accelerometers on the test article. To avoid this issue, measurement devices that do not physically contact the test article must be used. Additionally, accelerometers provide sparse information about mode shapes since they only acquire data at a few discrete points. One alternative method to measure vibrational responses of an object is Stereo Digital Image Correlation (DIC). Stereo DIC utilizes two high-speed cameras oriented towards the test article at specified angles to track the location of a group of speckle marks located on the test article [1]. Modal measurements with DIC can enable testing in high-shock environments; with hazardous materials such as Beryllium, or high explosives; or in testing large components which would otherwise require an excessive number of accelerometers to characterize [2]. DIC can even be used on small components where mass loading becomes a more prominent issue [3].

Previous comparisons between DIC and Laser Doppler Vibrometry (LDV) [4, 5] have shown that both technologies can produce similar results to those from traditional accelerometer measurements. It was found that LDV yields more precise out-of-plane results and equally precise in-plane results when compared to DIC. However, LDV lacks the strain measurements that DIC provides, which is useful for qualification testing. DIC can provide instantaneous full-field measurements in contrast to LDV and accelerometer measurements. Scanning LDV can perform full-field measurements, however, the process of scanning does not allow for time-dependent testing, such as shock testing with an impact hammer. Warren et al. having conducted impact tests, stated that DIC provides a distinct advantage over LDV in the measurement of rigid body motion and large vibrational displacements corresponding to lower frequencies [6]. Further investigations into the validity of DIC for modal analysis have pointed out that high frequency vibrations, which are easily detectable by accelerometers, may not displace above the noise floor for DIC, limiting the maximum frequency measurable [4]. Javh et al. introduced a hybrid DIC-accelerometer approach where an accelerometer is used to find the resonant frequencies and damping ratios, enabling DIC to find the high-frequency mode shapes utilizing full-field data after combining the Least-Squares Complex Frequency method and the Least-Squares Frequency-Domain method [7]. Most of the previous studies discussed here studied DIC for use in forced-normal-mode testing. There exists minimal research on using DIC for impact tests.

Through this study, our aim was to further investigate the viability of DIC measurements through a comparison to accelerometer measurements and preliminary Finite Element Analysis (FEA) models on a simple 6061-T6 aluminum plate. We performed free vibrational tests using a modal hammer to excite the plate and measured the plate's response as it rang down using both a calibrated DIC system and accelerometers. Due to the nature of impact testing, we simultaneously activated and analyzed multiple modes. This differs from previous studies where only one mode shape was analyzed at a time using forced-normal-mode-excitations. We used natural frequencies, mode shapes, and damping ratios to compare all measurement methods and the FE model.

Methods

Test Apparatus

The test article was an aluminum 6061-T6 plate with dimensions of 7 in by 8 in by 3/16 in, seen in Figure 1. The flat rectangular shape was chosen to simplify the comparisons between measurement methods and to avoid symmetric modes that would exist with a square plate. We opted to investigate the out-of-plane dynamics of the plate. The two top corners of the plate were connected with fishing line to a rigid mounting fixture, while the two bottom corners were loosely attached to the fixture with bungee cords to remove excess rigid body motion and keep the plate within the cameras' focus and field of view. In the finite element model, this mounting condition was approximated with free-free boundary conditions.

Finite Element Modeling of Plate Modes

We developed a model of the aluminum 6061-T6 plate within Abaqus to give a preliminary estimate of the mode shapes and natural frequencies of the plate. We performed a mesh convergence study, and the model was found to converge well using quadratic shell elements with seven integration points and an element size of 2.5 mm.

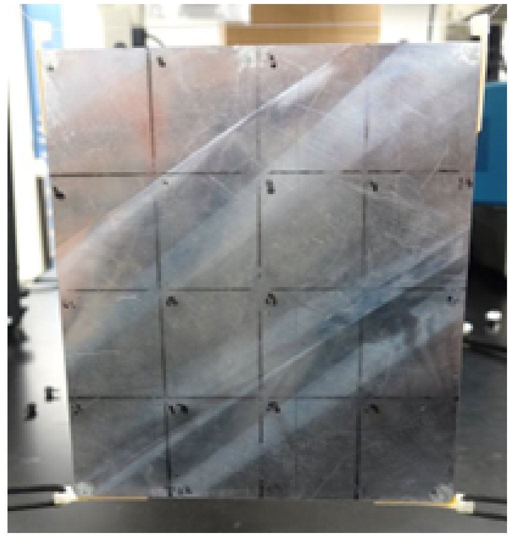

Fig. 1 Aluminum 6061-T6 rectangular test article

The first nine modes, shown in Figure 2, were used to compare DIC measurements and accelerometer measurements. Table 1 displays the natural frequencies associated with the first nine modes found by the FE model. These nine modes are all distinct, which allowed for clear confirmation on which modes we could identify within our experimental results.

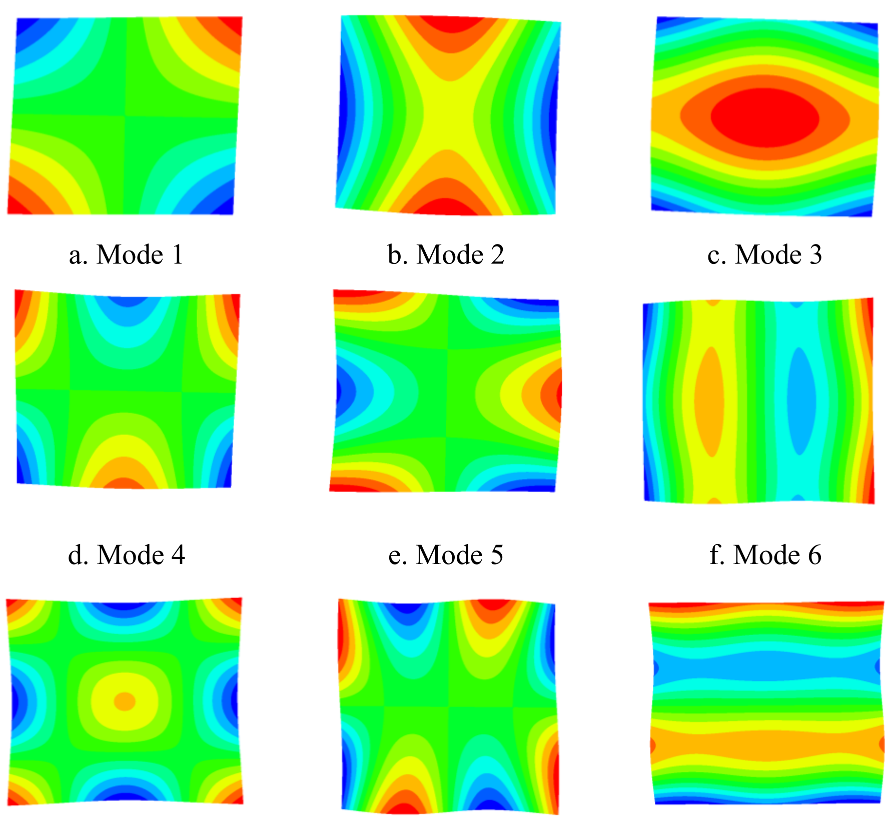

a. Mode 1 b. Mode 2 c. Mode 3

d. Mode 4 e. Mode 5 f. Mode 6

g. Mode 7 h. Mode 8 i. Mode 9

Fig. 2 Finite element model mode shapes

Table 1 Predicted natural frequencies from the finite element model.

Mode	1	2	3	4	5	6	7	8	9
Natural Frequency (Hz)	420	582	833	1040	1150	1710	1990	2070	2220

Accelerometer Setup

Using results from the FE model, we determined the optimal locations to mount five accelerometers. Locations were chosen to maximize the measured information about the first five mode shapes and therefore maximize our ability to distinguish between mode shapes from the accelerometer tests. To find the optimal accelerometer locations, we assigned a grid of 25 evenly spaced points on our Abaqus model as candidate locations and used the Effective Independence (EFI) method [8] to determine ideal accelerometer locations. EFI selected the four corners and the midpoint on the top edge of the plate, which we used as the accelerometer locations in our setup as shown in Figure 3.

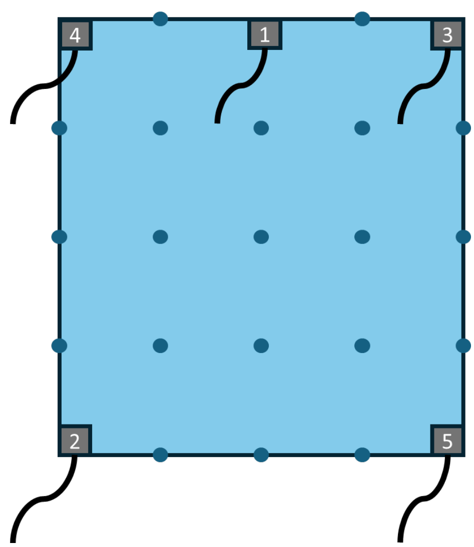

Fig. 3 Graphic of test article showing the grid of 25 candidate points and the optimized accelerometer placement based on EFI results

After mounting the accelerometers on the back side of the plate using modal wax, we performed a traditional roving hammer impact test by impacting the back of the plate at 25 points shown in Figure 3. For the 5 locations where accelerometers were attached, we impacted the front side of the plate to avoid directly impacting the accelerometers. A PCB Piezotronics SN22337 modal hammer was used to both trigger the DAQ and measure the impact force. Five PCB Piezotronics 356A01 triaxial accelerometers measured the output response after every hit. To sample from our sensors, we used a Siemens 16-channel LMS SCADAS Mobile DAQ and collected the sensor data with Simcenter Testlab.

DIC Setup

The experimental setup for DIC measurements is shown in Figure 4. To enable DIC measurements, we generated a random black and white speckle pattern in MATLAB and printed it on sticker paper. We applied the sticker paper to the face of the plate which faced the cameras. We mounted two color Photron Fastcam SA-Z high speed cameras to an optical breadboard and angled them at approximately 30° from each other. We fitted both cameras with a Canon 50mm lens set to an aperture of f/7.1, allowing an effective depth of field of approximately 42 mm for each camera, and ensuring that the plate would remain in focus during testing. We synchronized the cameras to each other by triggering them both via a single trigger input channel. To illuminate the test article during testing, we used two Veritas Constellation 120E lights with a maximum output of 12,700 lumens.

During testing, the impact hammer triggered both the cameras and the DAQ. Typically, the hammer operates at a constant 10 VDC, which briefly spikes during impact. To enable triggering of the measurement devices, we designed a custom circuit to remove the DC offset voltage and ensure the spike is large enough to trigger the devices, but not large enough to damage them. This circuit consisted of a buffer to avoid altering the measured hammer voltage, followed by a high pass filter to

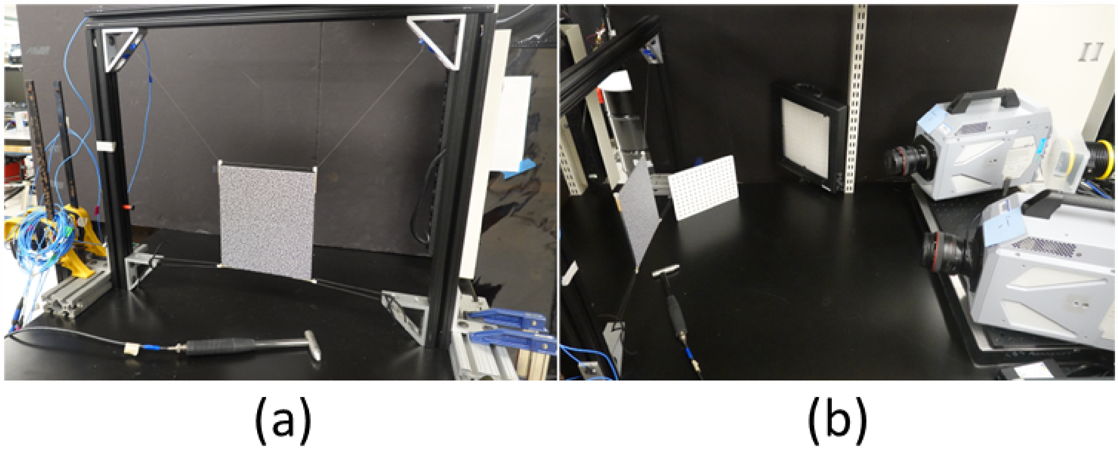

Fig. 4 Experimental test setup, including (a) the mounted test article and modal hammer used for excitation, and (b) cameras and lights pointed at the test article

remove the DC bias of the ICP voltage from the DAQ. Finally, the circuit amplified the signal to ensure the output voltage would exceed the 2.5 V trigger voltage recognized by the cameras and the DAQ. For the DIC recording, we set a pre-trigger of approximately 100 frames to capture the start of the impulse. To synchronize the timing of each measurement between hits, we applied a similar pre-trigger of the same length in Testlab.

We developed a workflow for conducting impact tests during a DIC recording to facilitate a comparison between DIC and accelerometer measurements. This method leveraged the use of the filter circuit so that successive hammer impacts would trigger separate DIC recordings which were partitioned within the camera's internal storage, allowing us to execute and record multiple impacts along the plate's surface. We triggered the DAQ using the same hammer impacts to simultaneously record the force data from the modal hammer, ensuring consistent and synced data recordings which could later be used in the development of Frequency Response Functions (FRFs). One limitation of this method was recording time. All impact events were stored on the camera's internal 64 GB memory, allowing for a total of 65,536 frames for the entire roving hammer test, assuming 8-bit color and 1 mega-pixel frames. It is possible to capture more frames by downloading images between hammer strikes; however, due to time constraints, we limited one full roving hammer test to the memory capacity of the cameras. Due to these recording limitations, we selected only 9 impact locations by excluding all edge impact locations. This increased the number of frames captured per hammer strike and minimized the probability of double-impacts which were more likely to occur on edge-impacts. An additional benefit to the reduced number of hammer strikes is that all strikes could be performed on the same side of the plate as the accelerometers, enabling testing with the accelerometers attached.

We recorded nominal DIC measurements at 5000 frames per second (FPS), which allowed for a total recording time of 13.1 seconds, or 1.46 seconds per impact location. To quantify mass loading caused by the attached accelerometers, we conducted two separate DIC tests: one test with attached dormant accelerometers, referred to as "DIC with mass loading", and one test without attached accelerometers, referred to as "DIC without mass loading". Additionally, to investigate the limits of frequency measurements and displacement resolution for our current setup, we conducted a third DIC test, referred to as "DIC at 10k FPS", with no accelerometers attached, at twice the frame rate of the previous tests, 10,000 FPS. For this test, we recorded only 4 impact locations, with 1.6 seconds per impact location. Because the image exposure time decreases as the frame rate increases, we were unable to increase the frame rate above 10,000 FPS with our current lighting setup. More lights, and/or brighter lights would enable higher frame rate recordings.

The processing steps are shown in Figure 5. First, we grayscaled the images and renamed them to be compatible with Vic-3D. Next, we processed the images in Vic-3D using the settings shown in Table 2. This yielded a series of Comma Separated Variable (CSV) files with information about the resonant response of the plate. We combined these files into one large CSV file containing only the out-of-plane displacement of each point at each time step. From this, we applied an exponential window to the displacement data, took the fast Fourier transform (FFT) at each point on the plate, and multiplied by $-\omega^2$ to convert to acceleration. We also applied the same window to and took the FFT of the hammer force data. With these frequency spectra, we used the H1 estimator method to calculate FRFs. Plotting the FRFs allowed us to locate the resonant frequencies of our plate. Additionally, we visualized the plate's mode shapes by plotting the modal vectors, the imaginary components of the FRFs at the resonant frequencies, on a 2D heat map.

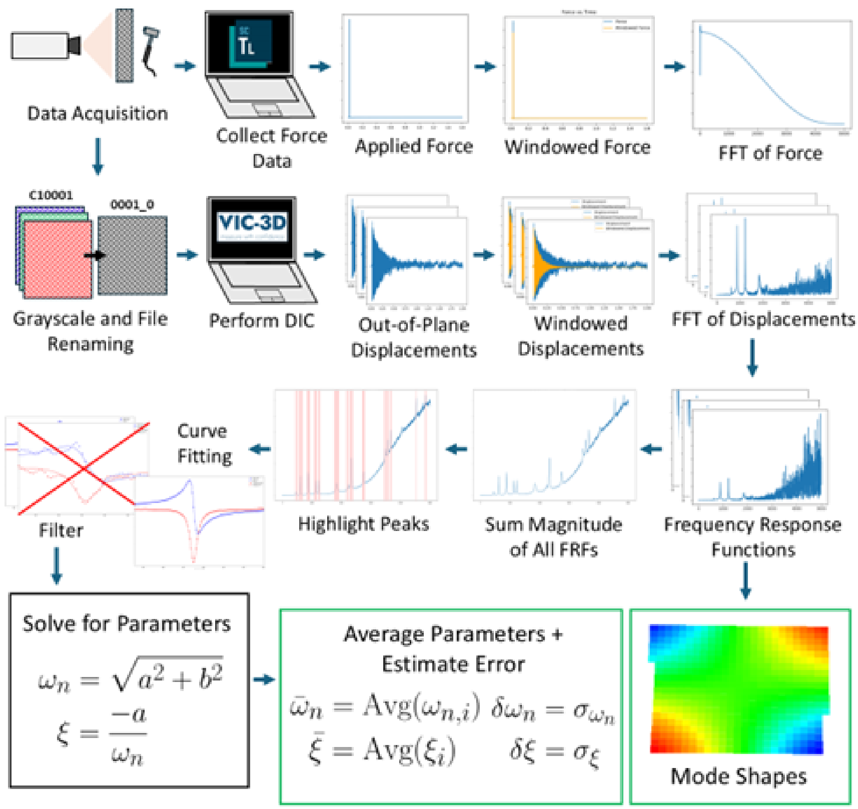

Fig. 5 DIC modal analysis workflow including data acquisition and the processing of both the camera and hammer data to extract modal information

Next, we plotted the sum of the magnitudes of the FRFs from each point on the plate and from each impact trial. This plot enabled us to highlight a region-of-interest around each peak so we could locally curve-fit to each peak in each FRF separately. We individually curve-fit the real and imaginary component of each peak in each FRF to the real and imaginary component of Equation 2.4.1, where A, B, a, b, $y_{0,Real}$, and $y_{0,Imag}$ are curve-fit parameters, ω is the independent variable frequency, i is the imaginary unit, and H is the transfer function. Each fit provided parameters which we used to calculate the damping ratio, ξ, and the natural frequency, ω_n, of the peak at that point for that trial, according to Equations 2.4.2 and 2.4.3 [9]. Poor fits were often caused by an FRF having a low signal-to-noise ratio for that peak, meaning the FRF contained little or no useful information about the modal parameters for that mode; therefore, we filtered out any results where the parameters a and b had an average standard error of greater than 5%. To estimate the damping ratio and natural frequency of a mode, we averaged together all the remaining results for that mode. We estimated our uncertainty in the damping ratio and natural frequency of each mode as the standard deviation of their corresponding distributions.

Table 2 Vic-3D settings used in this study.

Software setting	**Value**
Correlated solutions	Vic-3D v 9
Subset	39
Step size	30
Pixel size	0.2 mm/pixel
Minimization	ZNSSD
Interpolant	8-Tap
Image pre-filtering	None
Speckle size	1.25 mm

$$H = \frac{A + iB}{i(\omega - b) - a} + \frac{A - iB}{i(\omega + b) - a} + y_{0,\ Real} + iy_{0,\ Imag} \tag{1}$$

$$\omega_n = \sqrt{a^2 + b^2} \tag{2}$$

$$\xi = \frac{-a}{\omega_n} \tag{3}$$

Results and Discussion

Natural Frequency Results

To compare between measurement methods, one of the parameters we chose to investigate was our test article's natural frequencies. For FEA, we found the natural frequencies by conducting a frequency step analysis on our meshed model. For accelerometer testing, we used the roving impact hammer test described in Section 2.3 to collect data. Testlab produced FRFs and we conducted the post-processing steps described in Section 2.4 to find natural frequencies from a collection of FRFs. We used the steps described in Section 2.4, as opposed to Testlab's built-in post-processing, to ensure accelerometer and DIC data would be analyzed consistently. For DIC testing, we used the roving impact hammer workflow and post-processing steps described in Section 2.4 to find natural frequencies.

Figure 6 shows the difference between data from DIC and accelerometers for the first nine natural frequencies. The uncertainty from both accelerometer measurements and DIC measurements is propagated into the plotted percent differences.

For the DIC with mass loading test, there is very little discrepancy between measured natural frequency values for most modes, with absolute percent differences falling within a range of 0% to 1.635% and an average absolute percent

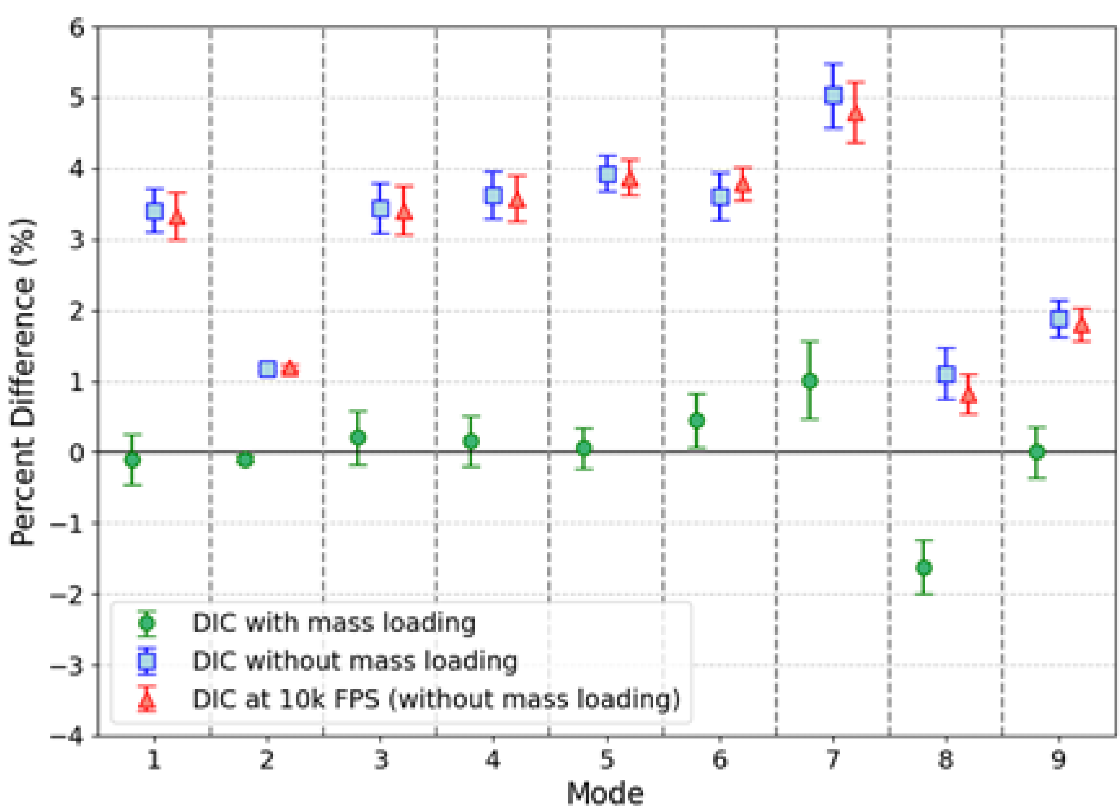

Fig. 6 Plot of percent differences of natural frequencies found using each DIC test from values found using the accelerometer test

difference of 0.414%. An outlier in this dataset was mode 8, which had a low signal-to-noise ratio (SNR) for the DIC with mass loading test. This caused zero curve fits to meet the filtering criteria during post-processing, so we chose to calculate modal parameters using only the best 1% of curve-fits as determined by the average standard error of their fit-parameters a and b. Aside from mode 8, there is a strong agreement between the accelerometer and DIC measurements of the natural frequencies.

On average, tests measured with DIC, with five accelerometers concurrently mounted, resulted in an average 3.017% lower natural frequencies than tests performed with DIC and no accelerometers mounted. We believe this offset is a result of mass loading caused by accelerometers. Tension and friction in the accelerometer cables could also contribute to the difference. There is strong agreement between the DIC test at 10K FPS and the DIC without mass loading, further supporting the hypothesis that mounted accelerometers alter the plate's natural frequency.

Table 3 Natural frequency measurements from FEA, accelerometers, and DIC.

	FEA	Accelerometer	DIC with mass loading	DIC without mass loading	DIC at 10k FPS
Mode	ω_n (Hz)	ω_n (Hz)	ω_n (Hz)	ω_n (Hz)	ω_n (Hz)
1	420	443 ±1	442.6 ±0.8	458.4 ±0.4	458.0 ±0.7
2	582	607.8 ±0.2	607.2 ±0.2	614.9 ±0.1	615.0 ±0.1
3	833	849 ±3	851 ±1	879.1 ±0.5	878.9 ±0.4
4	1040	1090 ±4	1092 ±1	1130.2 ±0.5	1129.7 ±0.3
5	1150	1184 ±3	1185 ±2	1231.8 ±0.4	1231.0 ±0.2
6	1710	1773 ±2	1780 ±6	1838 ±6	1841 ±4
7	1990	2082 ±8	2103 ±8	2189 ±5	*2184 ±4
8	2070	2220 ±6	*2184 ±6	2244 ±6	2238 ±2
9	2220	2288 ±5	2288 ±6	2332 ±3	2330 ±1
10	2580	2616 ±--	---	---	2748 ±2
11	3138	3340 ±--	---	---	*3474 ±1
12	3317	3497 ±--	---	---	*3559 ±8
13	3398	3634 ±--	---	---	*3670. ±4
14	3752	3859 ±--	---	---	*4061 ±7
15	4326	4447 ±--	---	---	*4543 ±6

* Curve-fitting filter criteria altered - Result may be unreliable.

Mode Shape Results

Mode shapes from FEA, accelerometer measurements, and DIC measurements were obtained and are visually compared. Accelerometer results were obtained using Testlab. Because we only sampled the plate at 25 hammer impact points, Testlab interpolated the amplitude between nodes to plot smoother mode shapes. DIC results were obtained using the steps described in Section 2.4. DIC's full field measurement yields mode shapes with higher resolution, so no interpolation was necessary to visualize the mode shapes. It is important to note that for accelerometer results, contributions from all impact locations on the plate contribute to the mode shape plots, while for DIC results, plots are taken from the highest amplitude peak across all impact events from a roving impact hammer test. Further work may be done to incorporate contributions from all impact locations with DIC testing, as well. Mode shape plots are qualitatively compared between various methods in Table 4.

From the various mode shapes shown in Table 4 we observe agreement between most modes from all measurement methods. FEA and accelerometer results show strong agreement throughout, while the noise of the DIC mode shapes increases as the frequency increases. This correlation is due to the higher frequency modes having a lower magnitude of displacement; the displacement magnitudes are close to the noise floor of DIC measurements. This effect is especially apparent in mode 8 because our DIC roving hammer test didn't impact any antinodes. When measuring with DIC the test article can be impacted with significantly more force than with accelerometers, due to the risk of damaging or overloading the sensors. This aided in resolving the higher mode shapes by increasing their deflection above the noise floor of DIC.

Overall, it is posited that if smoothing algorithms like ones used within Testlab were used, DIC results could obtain a higher qualitative agreement between all modes investigated. Future analysis would include the creation of cross-MAC matrices comparing all three measurement methods to get more objective and conclusive results.

Table 4 Mode shape plots from FEA, accelerometers, and DIC.

Mode	FEA	Accelerometers	DIC
1	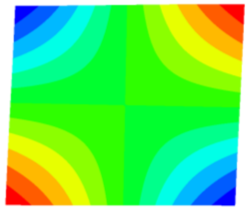	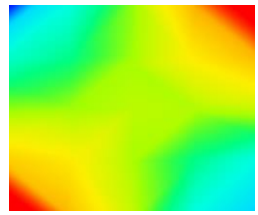	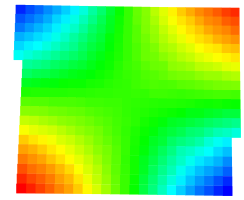
2	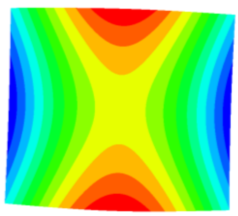	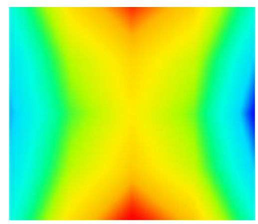	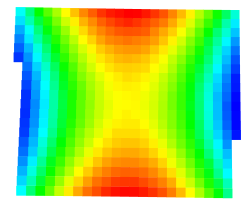
3	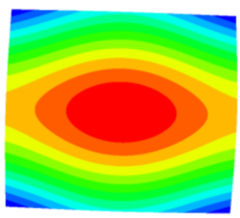	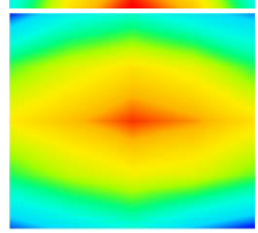	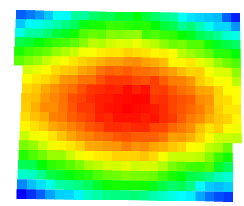
4	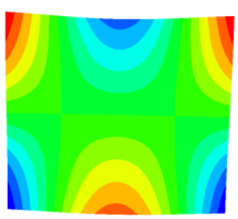	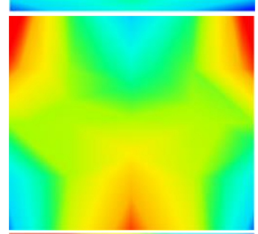	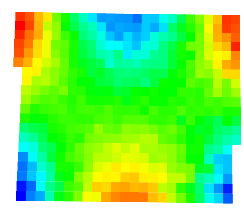
5	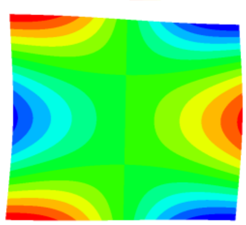	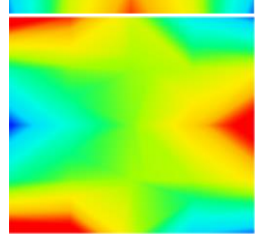	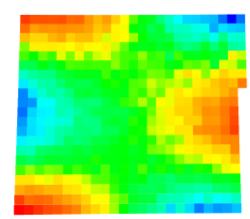
6	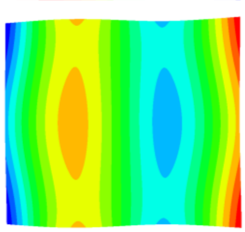	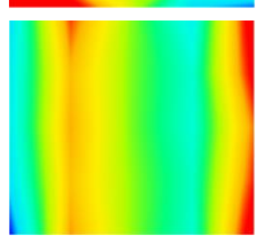	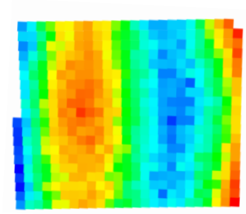
7	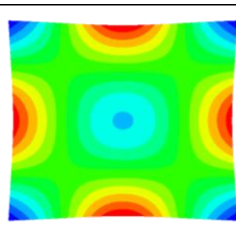	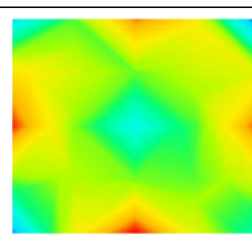	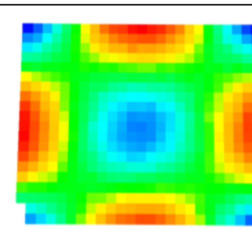

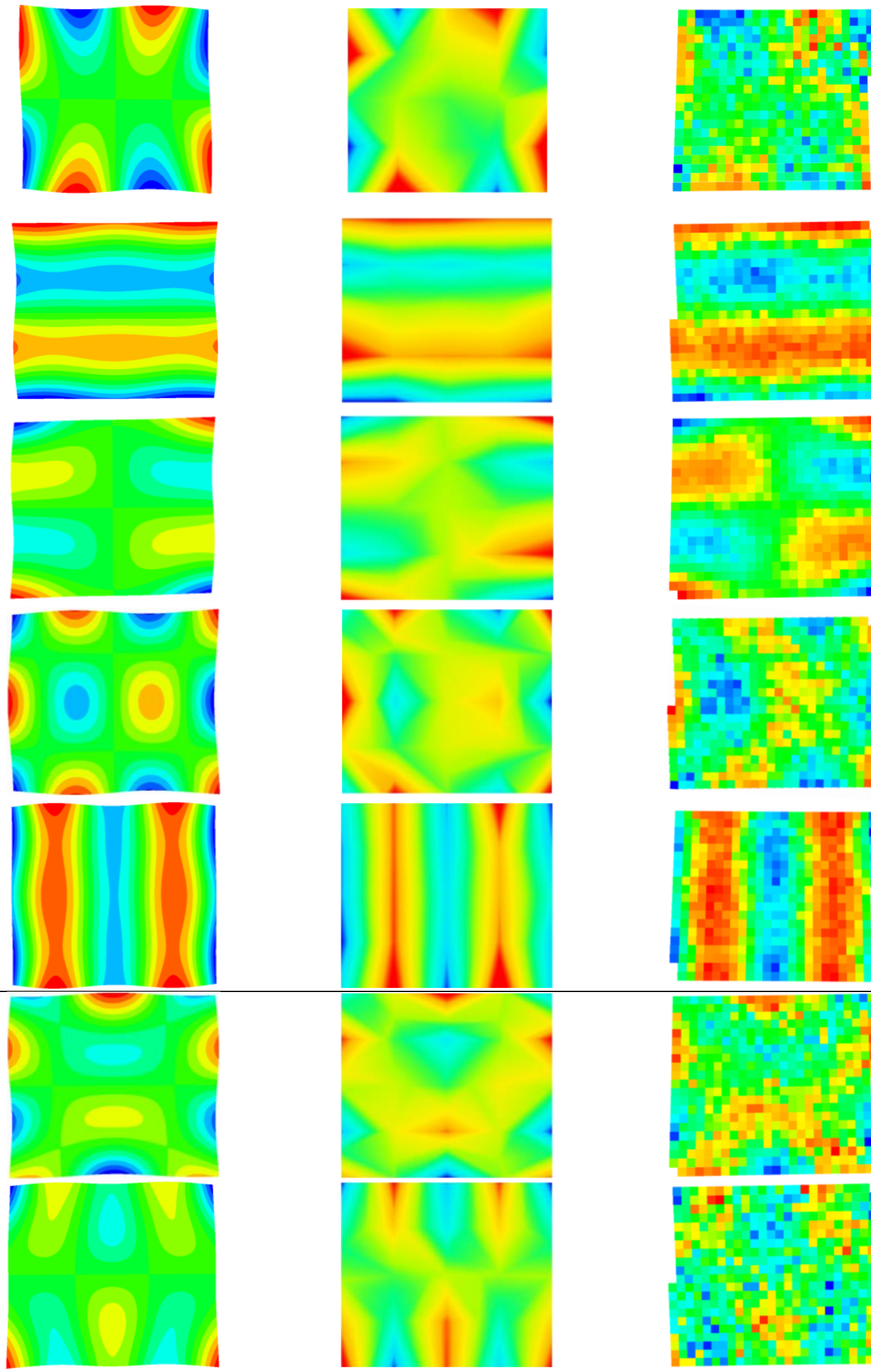

8

9

10

11

12

13

14

15	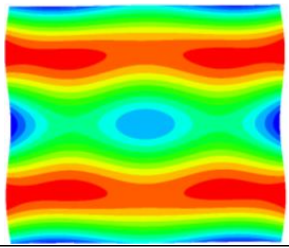	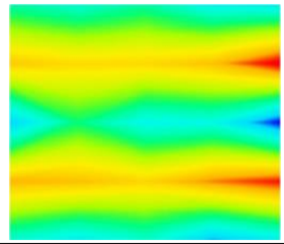	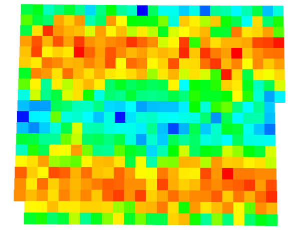

Damping Ratio Results

The final parameter we chose to compare was our test article's damping ratios. The methods for finding natural frequencies, described in Section 3.1, were also used for finding damping ratios from both accelerometer and DIC measurements.

To compare damping ratios, we created Figure 7 which shows the percent difference of the first nine damping ratios found using each DIC test from values found using the accelerometer test. We propagated the uncertainty from accelerometer measurements and DIC measurements into the plotted percent differences.

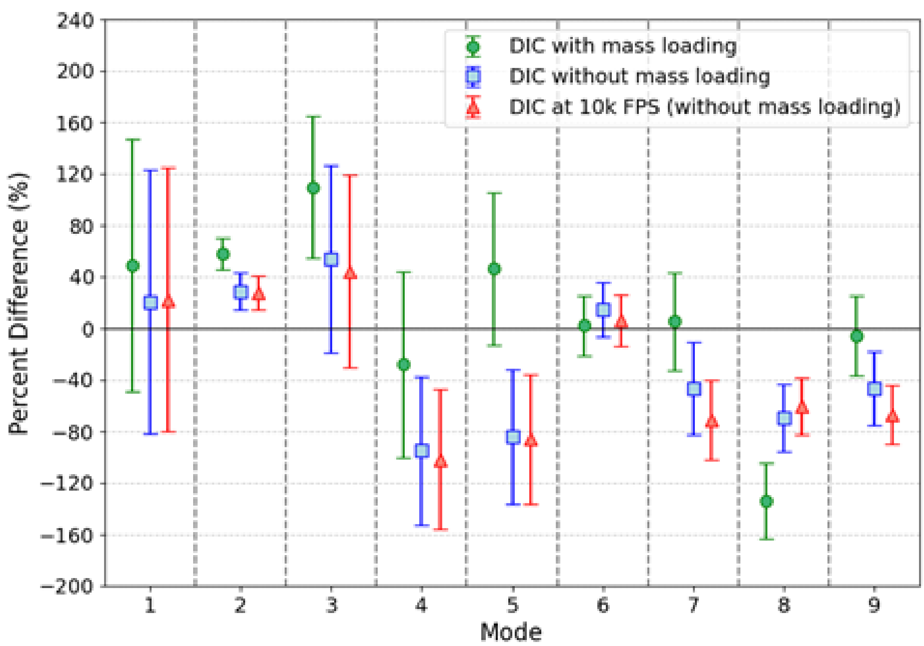

Fig. 7 Plot of percent differences of damping ratios found using each DIC test from values found using the accelerometer test

There was high variability when obtaining the values for damping ratios from different FRFs, resulting in large error bars as shown in Figure 7. The DIC with mass loading results tended to vary, either being less than or greater than the accelerometer baseline value. Due to this variability and the limited number of tests conducted, it is difficult to draw any specific conclusions comparing measurements conducted by accelerometers and DIC.

Our first hypothesis to explain the discrepancy between the accelerometer and DIC with mass loading measurements is that the addition of accelerometers can cause variability in the measured damping ratios. This is believed to not be caused by the mass loading itself but by the method by which the accelerometers are attached and the cable management associated with their attachment. PCB Piezotronics Model 080A109 petro wax was used as the mounting adhesive for experiments that required accelerometers. The accelerometer cables were secured with masking tape to prevent cable slap and tension during testing. However, it is still believed that the accelerometers may have introduced variable damping into the system. Further experiments would need to be conducted to either confirm or deny this hypothesis. Alternatively, the accelerometer measurements of damping ratios average results from all 25 impact locations, but the DIC measurements average results from hundreds of measurement locations. Since damping ratios may not be the same at all locations on a non-ideal test article, calculating results using different measurement locations would most likely yield different results. For the two DIC tests conducted without the presence of accelerometers, we see strong agreement between the results, demonstrating the repeatability of this measurement method. It shows that DIC measurements conducted during impact tests can be used to precisely measure damping ratios.

Table 5 Damping ratio measurements from accelerometers and DIC.

	Accelerometers	DIC with mass loading	DIC without mass loading	DIC at 10k FPS
Mode	ξ	ξ	ξ	ξ
1	0.010 ±0.008	0.013 ±0.002	0.010 ±0.001	0.010 ±0.002
2	0.0026 ±0.0003	0.0047 ±0.0003	0.0035 ±0.0003	0.0034 ±0.0002
3	0.010 ±0.002	0.011 ±0.001	0.0054 ±0.0005	0.0049 ±0.0005
4	0.008 ±0.007	0.007 ±0.001	0.0034 ±0.0005	0.0031 ±0.0003
5	0.009 ±0.004	0.010 ±0.001	0.0024 ±0.0005	0.0024 ±0.0002
6	0.007 ±0.001	0.012 ±0.002	0.014 ±0.002	0.013 ±0.002
7	0.017 ±0.005	0.016 ±0.003	0.009 ±0.002	*0.007 ±0.001
8	0.008 ±0.002	*0.002 ±0.001	0.005 ±0.001	0.0054 ±0.0009
9	0.009 ±0.002	0.007 ±0.001	0.0044 ±0.0009	0.0035 ±0.0004
10	0.0116 ±--	---	---	0.0039 ±0.0007
11	0.0069 ±--	---	---	*0.0036 ±0.0006
12	0.0023 ±--	---	---	*0.0018 ±0.0009
13	0.009 ±--	---	---	*0.0015 ±0.0008
14	0.0089 ±--	---	---	*0.0013 ±0.0007
15	0.0129 ±--	---	---	*0.0014 ±0.0004

* Curve-fitting filter criteria altered - Result may be unreliable.

Quantification of Mass Loading Effects

Recognizing that there could be differences between values as an effect of accelerometer inclusion or exclusion, we broke our tests into two distinct categories: with and without mass loading due to accelerometers being mounted. It was found that there was a distinct difference between the results of DIC tests that did and did not include attached accelerometers. This shows that there was a significant effect of mass loading caused by the accelerometers. This was most apparent in the natural frequencies where values tended to be relatively consistent between tests except when comparing mass loading scenarios. Here, as stated before, mass loading induced by accelerometers caused, on average, a decrease of 3.017% in the plate's natural frequencies. From damping ratios, it was also seen that there was a change caused by accelerometers. However, it is difficult to conclude the exact nature of the change, due to the large variability of results from tests with accelerometers attached. Further testing would likely lead to stronger conclusions.

Looking qualitatively at Figure 8, which shows an overlay of two FRFs between two DIC tests, one with and one without mass loading, we can see an apparent shift in natural frequencies and change in damping in the peaks. More specifically, the DIC with mass loading FRF shows a slightly lower resonant frequency for all the modes presented, which is consistent with the test article having a larger mass. The peaks of the FRF from the DIC without mass loading test tend to be more prominent with narrower widths indicating less damping. The increased damping that occurs in the DIC with mass loading tests comes from the added accelerometers along with the wax used to adhere them and the cables.

Tradeoffs Between DIC and Accelerometers

One of the benefits of DIC is its high spatial resolution. DIC can measure hundreds of points simultaneously which would require many accelerometers and DAQ channels to match. Additionally, using a high quantity of accelerometers can introduce even more significant mass loading and therefore can often be infeasible. This shortcoming of accelerometers is commonly addressed by attaching a small number of sensors and exciting the test article at many points and leveraging the reciprocity of linear systems to characterize the article's dynamics with higher fidelity. While this method requires few accelerometers,

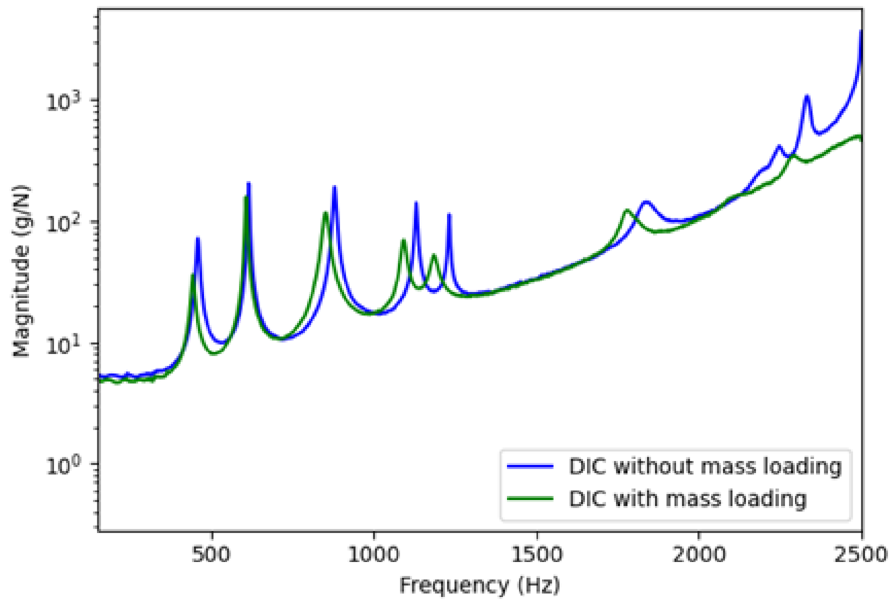

Fig. 8 Frequency response function plot from both DIC with and without mass loading

Table 6 Comparison of natural frequency and damping ratio measurements between DIC with and without mass loading.

	DIC with mass loading		DIC without mass loading		Percent difference	
Mode	ω_n (Hz)	ξ	ω_n (Hz)	ξ	ω_n %	ξ %
1	443.0 ±0.8	0.013 ±0.002	458. ±0.4	0.010 ±0.001	3.417	-26.09
2	607.8 ±0.2	0.0047 ±0.0003	614.9 ±0.1	0.0035 ±0.0003	1.161	-29.27
3	849 ±1	0.011 ±0.001	879.1 ±0.5	0.0054 ±0.0005	3.484	-68.29
4	1090 ±1	0.007 ±0.001	1130.2 ±0.5	0.0034 ±0.0005	3.621	-69.23
5	1184 ±2	0.010 ±0.001	1231.8 ±0.4	0.0024 ±0.0005	3.957	-122.6
6	1773 ±6	0.012 ±0.002	1838 ±6	0.014 ±0.002	3.600	15.38
7	2082 ±8	0.016 ±0.003	2189 ±5	0.009 ±0.002	5.010	-56.00
8	*2220 ±6	*0.002 ±0.001	2244 ±6	0.005 ±0.001	*1.075	*85.71
9	2288 ±6	0.007 ±0.001	2332 ±3	0.0044 ±0.0009	1.905	-45.61

* Curve-fitting filter criteria altered - Result may be unreliable.

it is more time-consuming. On the other hand, a standard DIC setup measures the test article with a high resolution simultaneously, requiring only a small amount of excitation points, which is conducive to short testing times. Multiple drive points are still required to sufficiently excite all the modes within the bandwidth of interest.

Another metric that is valuable to compare between DIC and accelerometers is temporal resolution or sampling rate which determines the measurable bandwidth. The cameras used for DIC have a maximum frame rate of 20,000 FPS. For this project, the maximum frame rate used was 10,000 FPS yielding a Nyquist frequency of 5000 Hz. The reason that we used a lower than maximum frame rate was because of lighting limitations. As camera framerate increases, shutter speed decreases, meaning less light is sensed by the camera. This means that at higher framerates, more illumination on the test article is required for the images to be clear enough for displacements to be measured. When we increased the framerate to above 10,000 Hz, our lights were insufficient for our cameras to capture the plate's dynamics.

A significant strength of DIC is the amount of data that it produces. This advantage can also be an obstacle. Especially while all the measurements are in the form of images taken by the cameras, the quantity of data is on the order of hundreds of gigabytes. As a result, the spatial, temporal and frequency resolutions that are possible during a test are all inversely proportional and are limited by the cameras' storage space, which in our case is 64 GB per camera. For example, a test recorded at 10,000 FPS on our cameras allows for 6.55 seconds of recording time. This means that assuming a test will use the cameras' entire memory, and that the spatial resolution is held constant, increasing the bandwidth of a modal test will decrease the frequency resolution.

One limitation of using accelerometers in an impact test is that excessive force can overload the accelerometers. With DIC this limit is removed. The main limit to applied force while using DIC is the force required to overload the force transducer. Additionally, the force should be low enough to not activate nonlinearities or to move the test article out of focus or frame. In our tests, we increased the force amplitude enough to ensure the plate's response would be above the noise floor.

An obstacle that we experienced in our DIC tests is that our setup had no anti-aliasing measures. When analyzing measured frequency responses, we had to question if we were seeing resonances outside of our Nyquist range. One strategy that we used to mitigate this issue was to select impact hammer tips that would excite frequencies within our bandwidth of interest and roll off after that. This method alone was not sufficient because there are only a few options for tip material, which limited control over hammer roll-off.

We were able to identify aliased modes in our data by comparing measured mode shapes that we expected were above Nyquist range to high frequency mode shapes in our FE model. Because of the high spatial resolution of the mode shapes measured by DIC, it was possible to identify features of modes well above our bandwidth of interest. In the high framerate test, we found an aliased mode and were able to identify its true frequency as shown in Figure 9. By knowing this mode was aliased, we could reflect the measured frequency of 4058 Hz about our Nyquist frequency of 5000 Hz to determine that this mode's resonant frequency was approximately 5942 Hz.

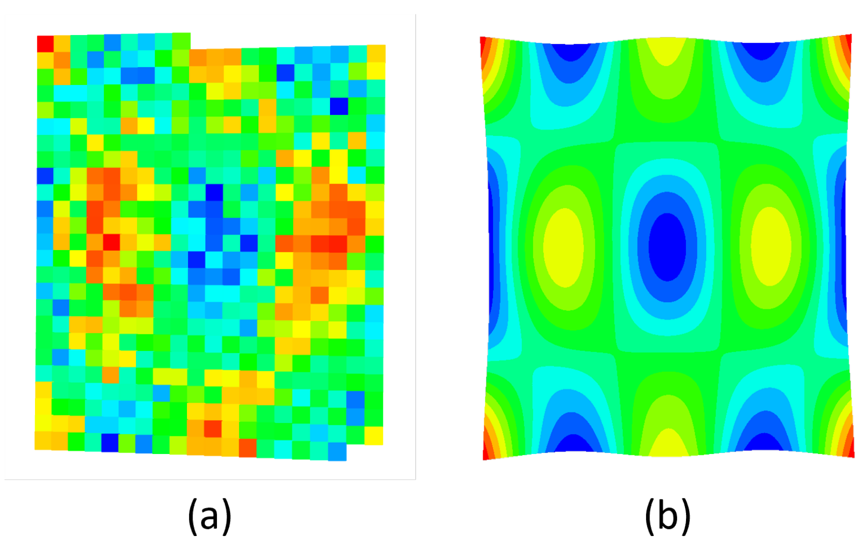

Fig. 9 (a) Aliased mode 18 measured by the 10k fps DIC test at 4058 Hz and (b) mode 18 modeled by the FEA at 5539 Hz. Reflecting about the Nyquist frequency, we measured this mode's resonant frequency to be 5942 Hz

Conclusions

By comparing measurements of impact tests using DIC and accelerometers we made multiple conclusions. We showed that natural frequency measurements of the article with accelerometers attached yield the same results with both measurement methods. Additionally, we qualitatively showed that mode shapes measured with DIC have higher resolution than with accelerometers but may have more noise. While there was a discrepancy between measurements of damping ratios between the two methods, we showed that DIC measurements have remarkable precision, regardless. This demonstrates that roving hammer impact tests measured with DIC have the potential to perform as well as accelerometers for determining modal parameters, especially at natural frequencies below 5000 Hz.

Furthermore, we showed that attaching accelerometers to our test article led to a significant alteration to the natural frequencies and damping ratios of our test article. We also suspect that attaching accelerometers increased the variability of damping ratio measurements. While DIC measurements without attached accelerometers showed remarkable consistency for all modal parameters, even with varying frame rates, damping ratio measurements didn't appear as consistent when accelerometers were attached. To confirm this conclusion, we would need to perform more DIC and accelerometer measurements of the test article with accelerometers attached. We suspect that external damping related to the wax, cables, and mass loading contributed to a general increase in damping ratios values and their variability.

Future Work

While this paper comparatively analyzes many aspects of DIC significant to its use in modal analysis, there is much opportunity for further research on DIC's advantages and limitations. We recommend testing DIC for modal analysis on test articles with more complex geometries than a rectangular plate. DIC can also be used for applications such as Resonant Ultrasound Spectroscopy, where minimal invasiveness and high-fidelity mode shape characterization is critical. Additionally, we recommend using DIC to quantify strain and modal parameters simultaneously during a high amplitude test for qualification testing.

Acknowledgments We would like to acknowledge the Los Alamos Dynamics Summer School leaders Shannon Danforth and Samantha Ceballes for their leadership and guidance through this project. This research was funded by and performed at Los Alamos National Laboratory (LANL) through the Engineering Institute's Los Alamos Dynamics Summer School. The Engineering Institute is a research and education collaboration between LANL and the University of California San Diego's Jacobs School of Engineering. This collaboration seeks to promote multidisciplinary engineering research that develops and integrates advanced predictive modeling, novel sensing systems, and new developments in information technology to address LANL mission-relevant problems. Los Alamos National Laboratory is an affirmative action/equal opportunity employer, and is operated by Triad National Security, LLC for the National Nuclear Security Administration of U.S. Department of Energy under contract no. 89233218CNA000001. The U.S. Government and the publisher, by accepting the article for publication, acknowledges that the U.S. Government retains a nonexclusive, paid-up, irrevocable, world-wide license to publish or reproduce the published form of this manuscript or allow others to do so, for U.S. Government purposes.

References

1. H. Schreier, J.-J. Orteu, and M. A. Sutton, "Image correlation for shape, motion and deformation measurements: Basic concepts, theory and applications," *Image Correlation for Shape, Motion and Deformation Measurements*, 2009.
2. R. Janeliukstis and X. Chen, "Review of digital image correlation application to large-scale composite structure testing," *Composite Structures*, vol. 271, p. 114143, 2021/09/01/ 2021, doi: https://doi.org/10.1016/j.compstruct.2021.114143.
3. B. Liu et al., "Digital image correlation in extreme conditions," *Thin-Walled Structures*, vol. 205, p. 112589, 2024/12/01/ 2024, doi: https://doi.org/10.1016/j.tws.2024.112589.
4. M. N. Helfrick, C. Niezrecki, P. Avitabile, and T. Schmidt, "3D digital image correlation methods for full-field vibration measurement," (in English), *Mech Syst Signal Pr*, vol. 25, no. 3, pp. 917-927, Apr 2011, doi: 10.1016/j.ymssp.2010.08.013.
5. P. L. Reu, D. P. Rohe, and L. D. Jacobs, "Comparison of DIC and LDV for practical vibration and modal measurements," *Mech Syst Signal Pr*, vol. 86, pp. 2-16, 2017/03/01/ 2017, doi: https://doi.org/10.1016/j.ymssp.2016.02.006.
6. C. Warren, C. Niezrecki, P. Avitabile, and P. Pingle, "Comparison of FRF measurements and mode shapes determined using optically image based, laser, and accelerometer measurements," *Mech Syst Signal Pr*, vol. 25, no. 6, pp. 2191-2202, 2011/08/01/ 2011, doi: https://doi.org/10.1016/j.ymssp.2011.01.018.
7. J. Javh, J. Slavič, and M. Boltežar, "High frequency modal identification on noisy high-speed camera data," *Mech Syst Signal Pr*, vol. 98, pp. 344-351, 2018/01/01/ 2018, doi: https://doi.org/10.1016/j.ymssp.2017.05.008.
8. J. E. T. Penny, M. I. Friswell, and S. D. Garvey, "Automatic choice of measurement locations for dynamic testing," *AIAA Journal*, vol. 32, no. 2, pp. 407-414, 1994, doi: 10.2514/3.11998.
9. C. W. Miller, "Determination of Modal Parameters from Experimental Frequency Response Data," 1978.